

# Correction of etaloning effects in ground-based hyperspectral image cubes of Jupiter

Erandi Wijerathna  
Klipsch School of Electrical  
and Computer Engineering  
New Mexico State  
University  
1305 Frenger St, Las  
Cruces, NM, 88001  
575-636-0510  
erandi@nmsu.edu

Emma Dahl  
Department of  
Astronomy  
New Mexico State  
University  
1320 Frenger Mall, Las  
Cruces, NM, 88001  
575-646-4834  
dahlek@nmsu.edu

David Voelz  
Klipsch School of Electrical  
and Computer Engineering  
New Mexico State  
University  
1305 Frenger St, Las  
Cruces, NM, 88001  
575-646-3471  
davvoelz@nmsu.edu

Nancy Chanover  
Department of  
Astronomy  
New Mexico State  
University  
1320 Frenger Mall, Las  
Cruces, NM, 88001  
575-646-2567  
nchanove@nmsu.edu

**Abstract**—The New Mexico State University Acousto-optic Imaging Camera (NAIC) at the Apache Point Observatory 3.5-m telescope is collecting narrowband hyperspectral image cubes of Jupiter from 470-950 nm during the perijove passes of the Juno spacecraft. For operations prior to 2018, the focal plane used for NAIC was a 1024x1024 pixel<sup>2</sup> backside illuminated, high quantum efficiency CCD. However, the narrowband images show evidence of “fringing”, due to “optical etaloning.” For much of our collected data, a flat-field correction successfully removes the fringing from the science images. However, for some absorption features, especially in Jupiter’s prominent CH<sub>4</sub> bands at ~890 nm, differences in the illumination spectrum of the flat-field source and Jupiter leave residual fringing in the images. Observation of the fringe pattern in the flat-field images as a function of wavelength suggested we could assume a thickness function with a single layer involving a single reflective surface. The thickness of the sensor has a “dish-shaped” variation as a function of pixel position in addition to finely spaced surface polishing marks. Using a mathematical interference (fringe) model, we were able to solve for the 2-D physical thickness function of the CCD at each pixel by minimizing the mean square error between the fringe model and the pixel spectral data. Synthetic fringe frames were created using the 2-D thickness function and scaled with best-correction contrast values. The flat-field and Jupiter images were corrected separately for fringing with division by the synthetic fringe frames. Fringe-corrected Jupiter frames are divided by fringe-corrected flat field frames to yield the final Jupiter science images, which show little evidence of etaloning.

## 1. INTRODUCTION

Optical etaloning is an interference effect that occurs when some of the light incident on the detector penetrates the sensor material and reflects off a rear surface or structure. The result is intensity variations or “fringes” superimposed on the detected signal. The intensities and the locations of the fringes are dependent on the wavelength and the thicknesses of the layers in the CCD [1]–[5]. In a thinned, back-illuminated CCD, as the Si absorption coefficient decreases with wavelength, the detection layer becomes more penetrative and causes the reflected intensity to be significant enough to produce discernible fringes [1], [3], [4]. For Si detectors, fringing becomes more prominent at wavelengths longer than ~700 nm [1]–[6]. Moreover, narrowband light results in higher-contrast fringes relative to broadband illumination as there is no spectral averaging of the fringes [3], [4]. In this paper, we describe and demonstrate an approach for the correction of etaloning effects found in narrowband spectral imagery of Jupiter collected with the New Mexico State University Acousto-optic Imaging Camera (NAIC) at the Apache Point Observatory.

Etaloning has been experienced in a variety of astronomical applications [1]–[4], [7]–[9] and has even occurred with the sensors on the Hubble Space Telescope [1], [4], [7], [9]. It can be mitigated by using sensors with thicker detection layers, but the thinned, back illuminated devices can have a significant advantage in quantum efficiency. The process of removing fringes after data collection is aptly named “defringing.” There are a few defringing approaches discussed in the literature [1], [3], [6], [8]. Malumuth et al. [1] suggested a method to develop a thickness function for the detection layer of the CCD using a Fresnel equation model. This method has been used to correct fringes in images from the Hubble telescope [2], [4], [7]. Even though these researchers used a limited number of images to support the model, they had prior knowledge of the structure of the CCD including its layers and nominal thicknesses. Howell [3] proposed a method to correct fringes of a star field by the use of flat-field frames obtained with illumination from a Neon lamp. This was possible in this case because the neon

## TABLE OF CONTENTS

1. INTRODUCTION .....	1
2. NAIC SYSTEM AND DATA COLLECTION .....	2
3. APPROACH.....	3
4. RESULTS AND DISCUSSION .....	5
5. CONCLUSIONS .....	7
ACKNOWLEDGEMENTS .....	7
REFERENCES.....	7
BIOGRAPHY .....	7

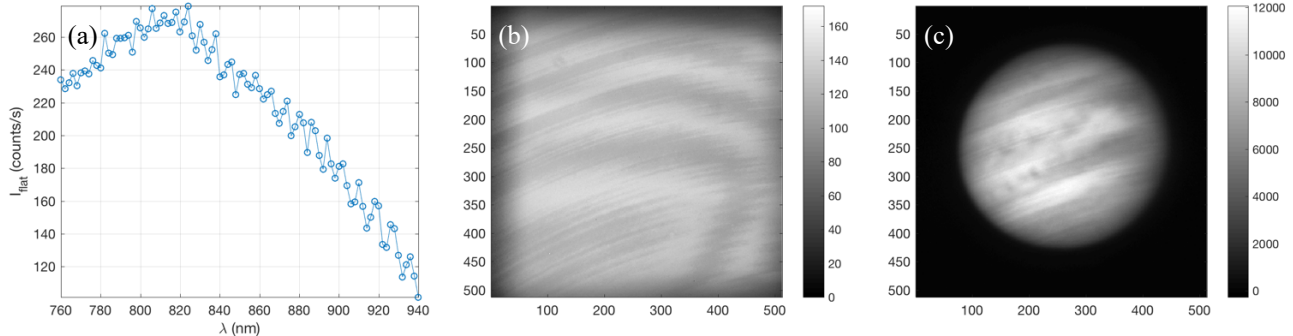


**Figure 1.** (a) Flat-field intensity at pixel  $(x, y) = (300, 200)$  as a function of wavelength, (b) a flat-field with

emission line source provides a match to the night-sky emission that produces the fringing. Rojo et al.[8] suggested a method based on wavelet transform and a local spectral technique, however, the method does not completely remove the fringes when the fringes in the frames are significant. Ren et al. [6] also suggested a wavelet-associated method to correct fringing in an interference imaging spectrometer. However, these methods are dependent on the application (e.g. observing a planet or a star constellation), prior knowledge of the CCD structure (e.g. constituent layers, nominal thicknesses) and the ability to collect more flat-field data.

## 2. NAIC SYSTEM AND DATA COLLECTION

The NAIC instrument collects narrowband hyperspectral image cubes of Jupiter from 470-950 nm at 2 nm intervals and has recently been operated with the Apache Point Observatory 3.5-m telescope during the perijove passes of the Juno spacecraft. The NAIC observations of Jupiter's uppermost cloud deck complement Juno's infrared and microwave observations. The NAIC utilizes an acousto-optic tunable filter (AOTF) operated with a radio frequency (RF) signal where the RF frequency selects the central wavelength of the narrowband filter. The average spectral resolving power of the filter is  $R = 242$ . For operations prior to 2018, the focal plane used for NAIC was a 1024x1024 pixel<sup>2</sup> (typically binned 2x2), backside illuminated, high quantum efficiency CCD, which shows evidence of etaloning.

It is pertinent to our discussion to describe two correction procedures applied to the NAIC science images. Since the AOTF separates the narrowband signal light angularly by

diffraction from broadband light, stray broadband light can be scattered into the narrowband path. This stray light component can be observed separately at the focal plane by switching off the RF drive signal to the AOTF. Thus, the stray light signal in the “RF-on” narrowband image of the planet is removed by subtracting a corresponding “RF-off” image. This procedure is analogous to a conventional dark frame correction. The second adjustment is a flat-fielding correction to remove spatial variations in the instrument’s response. Quartz lamps within the closed dome are used to produce uniform illumination at the focal plane. Images of this flat-field are collected at 2 nm intervals, corresponding RF-off frames are subtracted, and the resulting flat-field frames are normalized to a mean of one. The science frames are then divided by the corresponding flat-field frames.

The onset of etaloning fringes in the NAIC images is observed around 720 nm. Figure 1 (a) shows intensity as a function of wavelength for a single pixel  $(x, y)$  in a flat-field cube. The periodic signature of etaloning is apparent and it is superimposed on large slope features, peaking around 820 nm, that are due to a combination of the AOTF transmission response and the quantum efficiency response of the sensor. Figures 1 (b) and (c) show examples of a flat-field frame and a Jupiter image with etaloning effects at a wavelength of 868 nm. Several intensity features, particularly identifiable in the flat-field frame, suggest certain characteristics of the detector surface and layers. Large fringes, roughly curling around an area near the lower-left corner of the frame, are likely due to a “dish-shaped” thickness function between the sensor face and an internal layer. Smaller fringe-like features appear to be caused by polishing grooves on the top face. The grooves remain in fixed positions although their corresponding

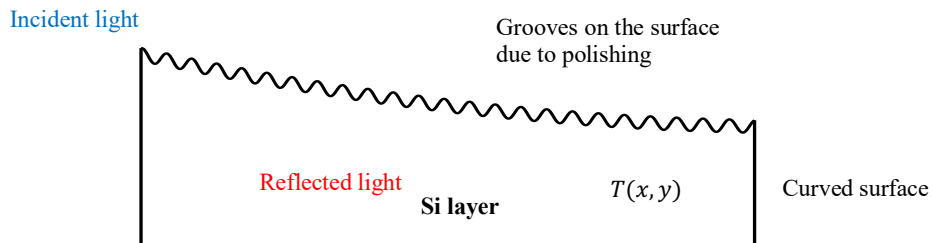


**Figure 2.** A cross section schematic of the Si layer of the detector.  $T(x, y)$  is the Si layer thickness at a pixel  $(x, y)$ .

intensities change as a function of wavelength. Other features in Figure 1(b) such as the loss of sensitivity at the edges and some horizontal banding are due to the transmission characteristics of the AOTF. A notional sketch of the detector cross-section is illustrated in Figure 2. As noted in section 4, reflections from other layers within the sensor likely contribute to further fringing but this surface and single layer contribution model appears to be effective for describing the primary etaloning effects.

Etaloning produces fringing in both the flat-field images and the Jupiter images. Therefore, it can be anticipated that the fringes in the science images can be corrected by the corresponding flat-field frame division. However, this is only true if the optical spectral content of the science source (e.g., Jupiter) is the same as the spectral content of the flat-field source (quartz lamps). As presented in section 4, for much of the wavelength range, the flat-field correction successfully removes the fringing from the science images. However, for some absorption features, especially in Jupiter's prominent methane ( $\text{CH}_4$ ) bands at  $\sim 890$  nm, differences in the illumination spectrum of the flat-field source and Jupiter leave residual fringing in the images. It is this residual fringing that we address in our correction approach.

The physical attributes of our commercial sensor are not available from the manufacturer. However, because the NAIC instrument provides a sequence of images at small wavelength steps, it is possible to deduce the thickness function from the flat-fields image spectral data. In this paper, we formulate an interference model based on wave optics field equations. Comparing the model with a sequence of flat-field images as a function of wavelength, we develop the 2-D physical thickness function of the CCD at each pixel. Based on the derived thickness function, we build a synthetic fringe model as a function of wavelength to correct fringes in the flat-field and Jupiter images. The method is entirely computational and no prior knowledge of the sensor schematics or further data collection is necessary.

### 3. APPROACH

Assuming flat-field illumination of a single thickness function formed by a surface and single layer, the field  $U(x, y; \lambda)$  and the intensity  $I(x, y; \lambda)$  pattern associated at a pixel  $(x, y)$  can be described by

$$U(x, y; \lambda) = 1 + \alpha(\lambda) \exp[-j2k(\lambda)n(\lambda)T(x, y)] \quad (1)$$

$$I(x, y; \lambda) = 1 + \alpha(\lambda)^2 + 2\alpha(\lambda) \cos(2k(\lambda)n(\lambda)T(x, y)) \quad (2)$$

where  $\lambda$  is the wavelength,  $T(x, y)$  is the thickness function,  $\alpha(\lambda)$  is related to the contrast of the fringes,  $k(\lambda) = 2\pi/\lambda$  is the wavenumber and  $n(\lambda)$  is the refractive index of the detection layer. Here, the field amplitude (and intensity) for the signal without fringing is normalized to 1.

The first step is to determine the thickness function of the CCD. However, it is not possible to use an analytical formula

for the thickness function because of sporadic changes in the fringe pattern, which imply some unpredictable variations in the thickness layers [1]. Therefore, it is necessary to calculate the thickness function for each pixel in the detector.

#### Thickness function

A direct search approach was used to determine the thickness function. For a considered pixel, the intensity was extracted from the flat-field frames for the wavelength range of 820 to 940 nm (61 values), which corresponds to a linearly-sloped response region (see Fig. 1(a)). The slope was removed by a low pass filter. Next, we searched for the thickness value over a range of 5 to 30  $\mu\text{m}$  in 1 nm intervals by computing the intensity in Eq. (2) for a selected thickness for each wavelength in the range and calculating the Mean Square Error (MSE) between the computed intensity and the filtered flat-field intensity. The thickness value that produced the minimum MSE was chosen to be the thickness at the considered pixel. This was repeated for all pixels to obtain the 2D thickness function of the CCD. Figure 3 shows an example plot of the MSE vs. thickness value for a particular pixel. The MSE behaves in an oscillatory manner, which can result in some uncertainty in the selection of the definitive minimum value, but the minimum is clearly near 14  $\mu\text{m}$ . The 5  $\mu\text{m}$  to 30  $\mu\text{m}$  search range was chosen because the thickness of most thinned commercial CCDs falls in this region.

When applying Eq. (2) to find the thickness,  $\alpha$  was chosen to be the root mean square (RMS) value of the filtered signal for the particular pixel, although we found the choice of  $\alpha$  was not critical for finding the MSE. Even though the refractive index value of Si ( $n$ ) is a function of wavelength, we used a constant refractive index value  $n = 3.7$ , to simplify the calculation and because different references provide slightly different functions for the refractive index [1]. Also, the Si detection layer may consist of dopants and other impurities which can lead to further changes in the refractive index [1], [2].

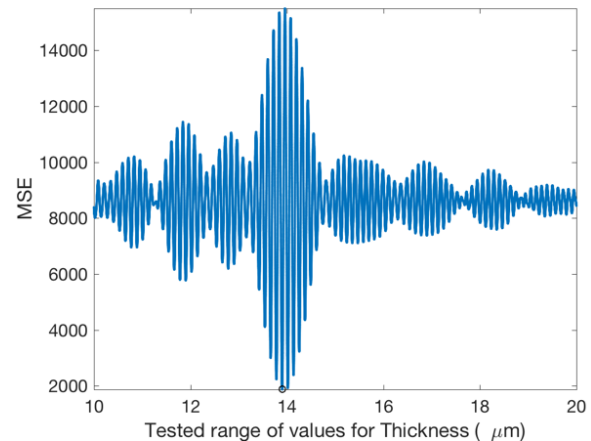


**Figure 3. Behavior of MSE for a range of . Black circle indicates the thickness value**

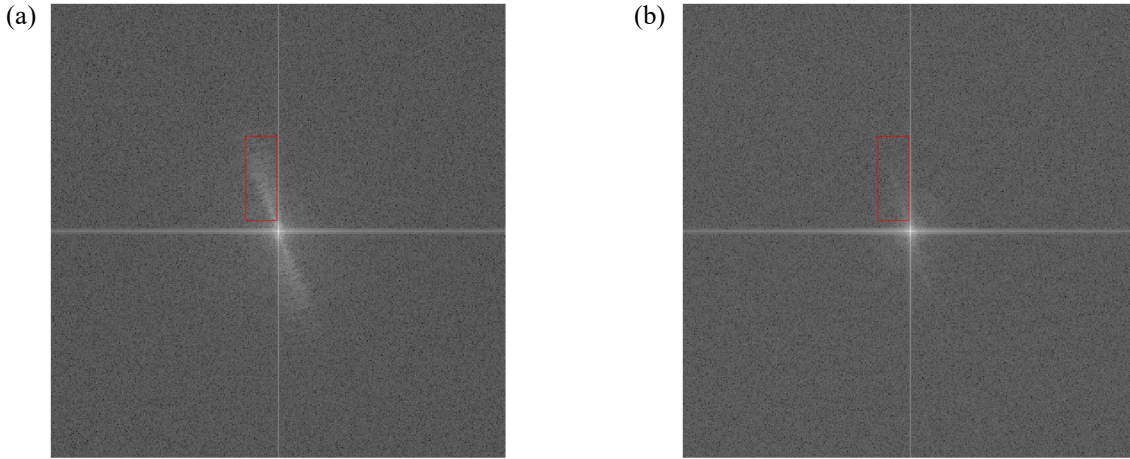


**Figure 4.** Power spectrum of (a) a fringe flat-filed and (b) the flat-field divided by the synthetic fringe frame.

#### Correction for etaloning

The first step in correcting the Jupiter images for the etaloning effects involves removing the fringes from each science frame and flat-field frame separately. Correcting the Jupiter and flat-field images separately compensates for the issue that the frames may have been formed with different optical spectral content. Fringing is removed by dividing the frame of interest by a normalized synthetic “fringe frame” that is created with the derived 2-D thickness function. A critical step is a search for the contrast values ( $\alpha$ ) that minimize the presence of the fringes in the flat-field frames and the science frames, respectively.

Our metric for determining the amount of fringing in a given frame is to compute the 2-D power spectrum of the frame and examine a portion of the power spectrum that corresponds to the fringing. Figure 4(a) shows a gray-scale representation of the power spectrum for a flat-field image where the tilted “bow-tie” feature is a signature of the fringing in our

particular CCD. Normalized synthetic fringe frames for a range of  $\alpha$ -values were created with the 2D thickness function applied to Eq. (2). The flat-field frame was divided by each synthetic frame trial and the resulting power spectra are monitored. The  $\alpha$  for the best correction was found when the fringe signature was minimized. The search range for  $\alpha$  was from  $-0.3$  to  $0.5$  at intervals of  $10^{-6}$ , although the contrast is typically less than  $0.025$  (2.5%). The negative values for  $\alpha$  were searched as we found that sometimes a slight phase reversal of the synthetic fringe pattern gave the best result. Figure 4(b) shows the power spectrum result for the example flat-field frame after dividing by the synthetic fringe frame with the best-correction contrast. This correction procedure was applied individually to all the flat-field frames over the wavelength range to get the best-correction contrast ( $\alpha_{flat}$ ) as a function of wavelength.

Next, the same steps were repeated for Jupiter images to determine the best-correction contrast ( $\alpha_{Jupiter}$ ) for the

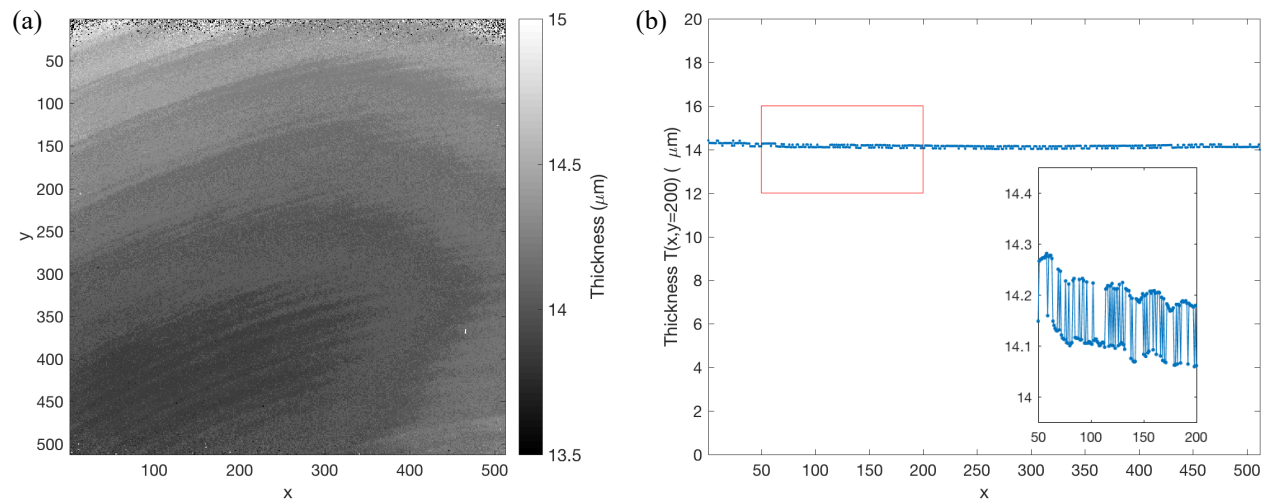


**Figure 5.** Thickness function obtained by minimizing MSE (a) 2-D profile and (b) 1-D cross sectional profile at  $y = 200$  and the inset is a magnification of the section marked by the red box.

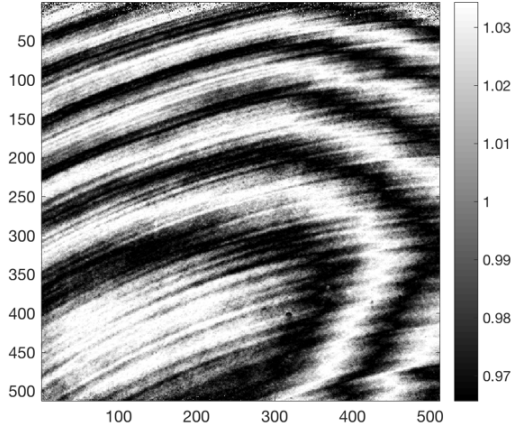


**Figure 6. Synthetic fringe pattern derived nm and**

synthetic fringe frames as a function of wavelength, although more care needs to be taken when examining the power spectrum to avoid components associated with Jupiter. The fringe-corrected Jupiter image is obtained by dividing by the appropriate synthetic fringe frame. The final science image is the fringe-corrected Jupiter image divided by the associated fringe-corrected flat-field image.

#### 4. RESULTS AND DISCUSSION

##### *Thickness function*

Figure 5(a) shows a gray-scale representation of the 2-D thickness function obtained with our approach. The arrangement of the contours is consistent with the fringe characteristics in Figure 1(b). An interesting aspect of Figure 5(a) is a slight “oscillation” of the thickness function that is spatially correlated with the 2-D contours. We believe this feature may arise because of a secondary reflection that is not

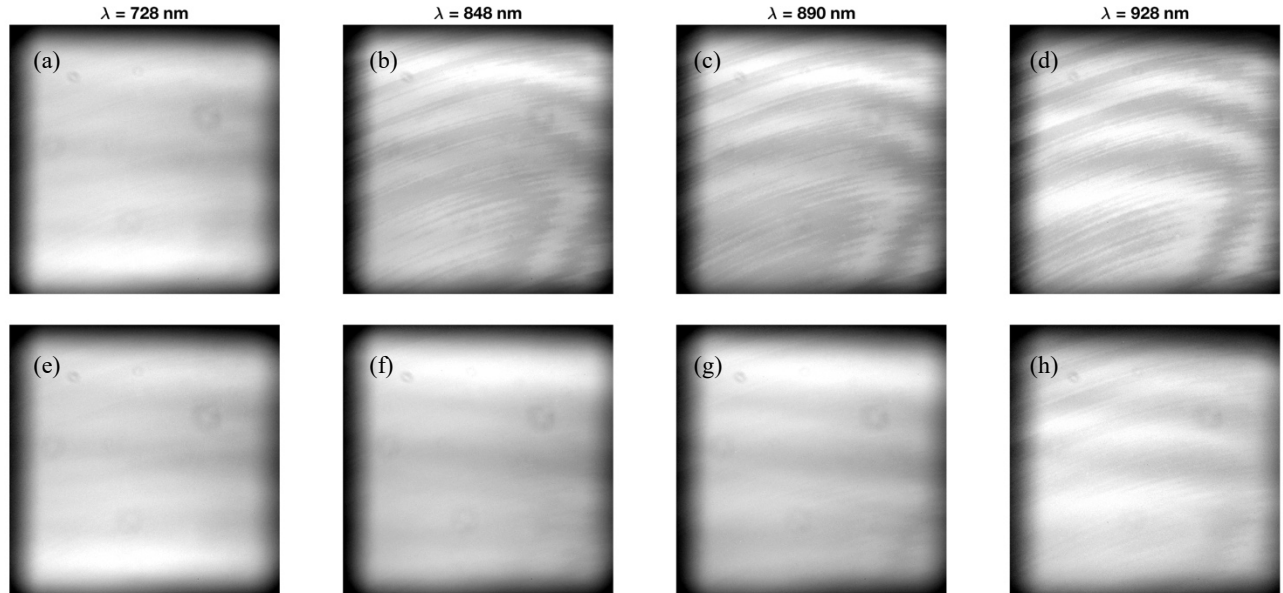
directly modeled by Eq. (2). We investigated this issue by simulating fringe frames with a two-layer system and then applying our method to solve for a single layer thickness. The results gave a thickness function with a similar oscillation feature. Ultimately, the image correction results suggest that although the single reflection model may not yield an exact physical representation of the CCD thickness function, it produces synthetic fringe frames that are a close match to the actual etaloning fringe patterns.

A 1-D profile of the thickness function in Figure 5(b) indicates a mean value of about  $14 \mu\text{m}$  and a slight downward curve and slope from left to right. The inset box in the figure shows the thickness value tends to jump between two levels. This ambiguity is due to the highly oscillatory nature of the MSE result for the thickness search. Due to noise, the minimum MSE can jump between two adjacent valleys. The maximum variations of these jumps are  $<1\%$  of the mean thickness and do not appear to significantly affect the results.

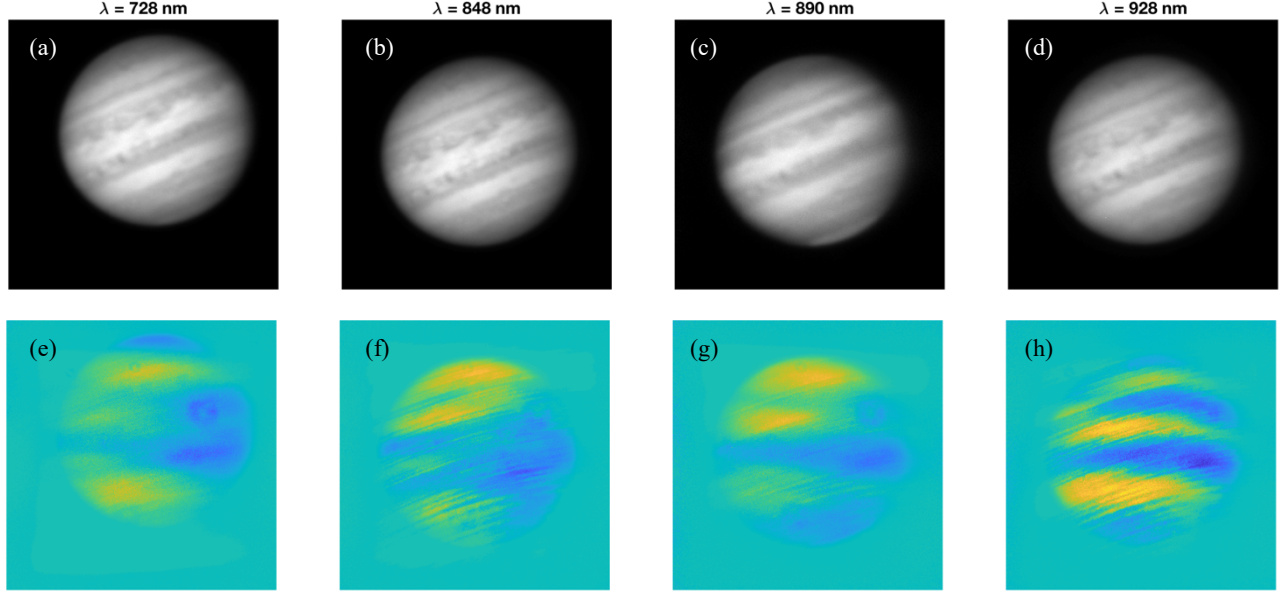
##### *Corrected images*

Figure 6 shows an example of a synthetic fringe frame obtained with Eq. (2) and the derived thickness function in Figure 4(a). The synthetic fringes appear similar to the fringes seen in the flat-field frame of Figure 1(a).

Examples of flat-fields images for four different wavelengths are shown in Figure 7. These examples represent the onset of fringes (728 nm), before and around one of the  $\text{CH}_4$  absorption regions of Jupiter (848 nm and 890 nm) and near the end of our data collection range (928 nm). The top row shows the frames with no correction and illustrates that the fringe contribution is minimal for 728 nm but becomes more pronounced as the wavelength increases. The bottom row shows the frames after correction and demonstrates the fringes removal. A few residual fringe contributions are apparent in the corrected 928 nm frame. The horizontal



**Figure 7. Examples for correcting fringes in flat-field images, Left-to-right in each row:  $\lambda = 728 \text{ nm}$ ,  $848 \text{ nm}$ ,  $890 \text{ nm}$  and  $928 \text{ nm}$ . (a-d) fringe flat-fields, (e-h) fringe corrected flat-fields using synthetic fringe frames.**



**Figure 8.** Examples for correcting fringes in Jupiter images, Left-to-right in each row:  $\lambda = 728 \text{ nm}$ ,  $848 \text{ nm}$ ,  $890 \text{ nm}$  and  $928 \text{ nm}$ . (a-d) fringe corrected Jupiter images using synthetic fringe frames and divided by the fringe corrected flat-fields, (e-h) difference between the original Jupiter images and the final corrected Jupiter

banding and other spot-like artifacts in the corrected frames are due to the AOTF transmission response. It is these response-related artifacts that are corrected in the Jupiter images with division by the flat-field frames.

Figure 8 presents example results for the Jupiter images. The top row shows the final science frames where fringe and flat-field corrections have been completed. Even in uncorrected-Jupiter frames, it can be difficult to identify fringing and transmission response artifacts because of the details in the planet. Therefore, in the bottom row of Figure 8, we show the difference between the final science frames and the original uncorrected Jupiter frames. These difference maps illustrate the combination of etaloning and flat-field artifacts that are removed from the Jupiter images.

It is interesting to plot the contrast values  $\alpha_{flat}$  and  $\alpha_{Jupiter}$  as a function of wavelength (Figure 9). For  $\lambda < 700 \text{ nm}$ , there are no obvious fringes in the flat-field or Jupiter images, therefore, the contrast values for both are close to zero. As the wavelength increases ( $\lambda > 720 \text{ nm}$ ), fringes appear and the  $\alpha$  values become larger. Note that when  $\alpha_{flat}$  and  $\alpha_{Jupiter}$  have comparable values for a particular wavelength, it indicates that the fringe patterns in both the flat-field and Jupiter frames are similar and correction of the science frames could likely be done with a conventional flat-field division. However, around the  $\text{CH}_4$  absorption region ( $\lambda \sim 890 \text{ nm}$ ),  $\alpha_{Jupiter}$  falls below  $\alpha_{flat}$ . This implies that for these wavelengths, the optical spectral content of the flat-

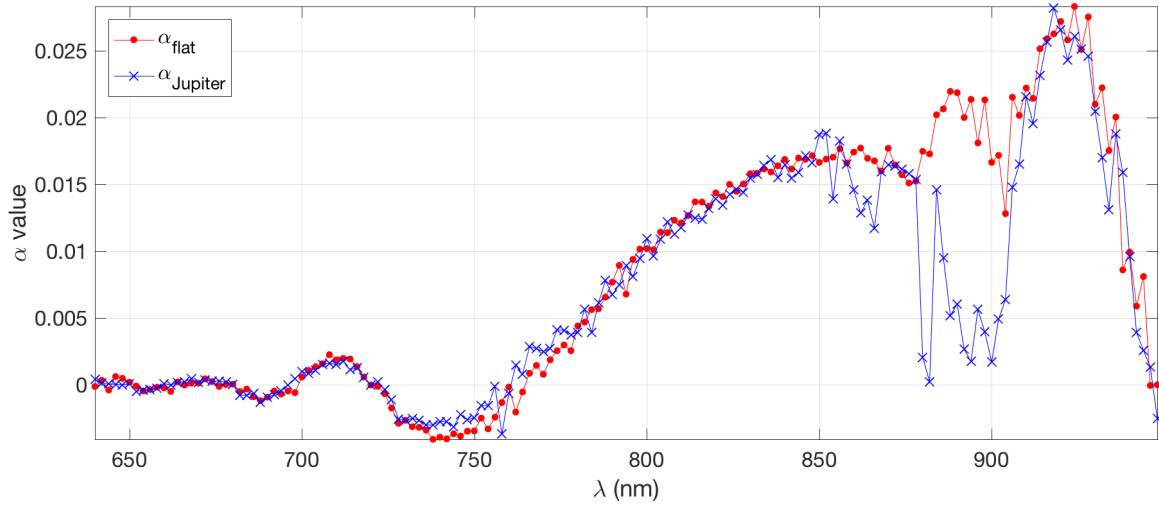


**Figure 9.** Best-correction fringe contrast ( $\alpha$ ) for creating synthetic fringe frames.

field over the AOTF bandpass differs appreciably from Jupiter's spectral absorption features.

## 5. CONCLUSIONS

In conclusion, we have developed a method to derive a 2-D physical thickness function of the CCD from a sequence of flat-field spectral images collected by NAIC. The method is based on wave optics field equations and assumes a single layer with a single reflective surface. Synthetic fringe frames were created using the 2-D thickness function and scaled with the best-correction contrast values. Each flat-field and Jupiter image was corrected separately by dividing by the associated synthetic fringe frames. The final science images, which are the fringe corrected Jupiter frames divided by the fringe corrected flat field frames, show significant reduction in etaloning fringe effects even at wavelength regions involving absorption features in Jupiter's optical spectrum. We expect this method is transferrable to other detectors when a sequence of flat-field spectral images with reasonable wavelength resolution is available.

## ACKNOWLEDGEMENTS

This work is supported by Research Support Agreement 1569980 from the Jet Propulsion Laboratory, as a subaward of a NASA/Solar System Observations grant.

Sincere thanks to Michael Wong at UC Berkeley for helpful discussions on etaloning and modeling the fringing.

## REFERENCES

- [1] E. M. Malumuth *et al.*, "Removing the Fringes from Space Telescope Imaging Spectrograph Slitless Spectra," *Publ. Astron. Soc. Pacific*, vol. 115, no. 804, pp. 218–234, 2003.
- [2] J. R. Walsh, W. Freudling, N. Pirzkal, and A. Pasquali, "Modelling the fringing of the ACS WFC and HRC chips," 2003.
- [3] S. B. Howell, "Fringe Science: Defringing CCD Images with Neon Lamp Flat Fields," *Publ. Astron. Soc. Pacific*, vol. 124, no. 913, pp. 263–267, 2012.
- [4] H. Wong, Michael, "Amplitude of fringing in WFC3 /UVIS narrowband red filters," 2010.
- [5] M. Kümmel, J. R. Walsh, N. Pirzkal, H. Kuntschner, and A. Pasquali, "The Slitless Spectroscopy Data Extraction Software aXe," *Publ. Astron. Soc. Pacific*, vol. 121, no. 875, pp. 59–72, 2009.
- [6] W. Ren *et al.*, "Wavelet transform based defringing in interference imaging spectrometer," *Opt. Express*, vol. 25, no. 15, pp. 17039–17050, 2017.
- [7] E. M. Malumuth *et al.*, "Model of Fringing in the WFC3 CCDs," in *Proc. SPIE 4854, Future EUV/UV and Visible Space Astrophysics Missions and Instrumentation*, 2003, pp. 567–576.

- [8] P. M. Rojo and J. Harrington, "A Method to Remove Fringes from Images Using Wavelets," *Astrophys. J.*, vol. 649, no. 1, pp. 553–560, 2006.
- [9] A. A. Simon, M. H. Wong, and G. S. Orton, "First Results From the Hubble Opal Program: Jupiter in 2015," *Astrophys. J.*, vol. 812, no. 1, p. 55, 2015.

## BIOGRAPHY



**Erandi Wijerathna** is a Ph.D. candidate in the Klipsch School of Electrical and Computer Engineering at New Mexico State University. Her research interests include laser beam propagation through atmospheric turbulence, image processing and polarimetric lidar. She earned a BS (Honors) in Physics from University of Colombo, Sri Lanka in 2011. She received her MS degrees in physics and in electrical engineering in 2016 from New Mexico State University.



**Emma Dahl** received her B.A. in Physics-Astronomy from Whitman College in 2015. She is currently a Ph.D. candidate in the New Mexico State University Astronomy Department, where she studies and observes Jupiter's atmosphere in support of NASA's Juno mission. Her other research interests include instrumentation and mission planning and design.



**David Voelz** is a professor in the Klipsch School of Electrical and Computer Engineering at New Mexico State University. He has been involved in the development of optical systems involving AOTF components since 2002. His research interests include spectral and polarization sensing, laser beam propagation through turbulence, astronomical instrumentation development, laser communications, and imaging theory. He earned a Ph.D. EE degree from the University of Illinois in 1987.



**Nancy Chanover** received her B.A. in physics from Wellesley College in 1991 and a Ph.D. in astronomy from New Mexico State University in 1997. She is currently a Professor of Astronomy at New Mexico State University. Her current research activities include the development and advancement of novel technologies for remote sensing and *in situ* applications in studies of solar system atmospheres and surfaces.